Early detection of stator voltage imbalance in three-phase induction motors

Rohan Samsi, Asok Ray*, Jeffrey Mayer

The Pennsylvania State University, University Park, PA 16802, United States

ARTICLE INFO

ABSTRACT

Online health monitoring of electric motors is of paramount interest to various applications. As the operation of industrial processes becomes more complex, the cost of health monitoring increases dramatically. To this end, much efforts have been directed towards enhancement of fault diagnostics and prognostics in electric motors, largely based on conventional signal processing and pattern classification. This paper formulates and experimentally validates a recently reported technique, called Symbolic Dynamic Filtering (SDF), for early detection of stator voltage imbalance in three-phase induction motors. The SDF-based imbalance detection algorithm is built upon the principles of wavelet transforms and symbolic time series analysis.

© 2008 Elsevier B.V. All rights reserved.

1. Introduction

Advanced automation and process integration in modern engineering facilities have placed stringent demands on reliability and performance of electric motors. To this end, several online fault monitoring techniques of varying complexity have been developed and deployed. Examples of the relatively simple techniques include *Negative Sequence Detectors* [1], *Kappa Transforms* [2], *Voltage Mismatch Detectors* [3,4]. More advanced techniques of pattern classification have also been used, for example, *Mechanical Vibration Monitoring* [5], *Signal Spectral Analysis* [6], and *Fuzzy Logic and Neural Networks* [7,8]. These techniques have their respective shortcomings and advantages; in general, simple techniques do not provide sufficiently early warnings, while advanced techniques require excessive computational resources.

This paper presents a computationally efficient and robust method for early detection of anomalies due to stator voltage imbalance in three-phase induction motors, where an anomaly is defined as a deviation from the nominal expected behavior of machine dynamics. Based on the observed anomalies, signal processing for fault detection is classified in two categories: (i) identification of signal features that have a high degree of correlation with one or more types of anomalies; and (ii) application of a decision-making algorithm to classify the set of measured signal features to identify a particular type of anomaly or the absence of an anomaly. These two categories may not be clearly distinguishable in many fault detection and identification techniques such as neural networks [8].

From the above perspectives, anomaly detection is posed as a two-time-scale problem as seen in Fig. 1. Time series data of measured variable(s) are collected in the fast time scale at discrete slow-time epochs, over which progression of anomalies may take place in the form of parametric or non-parametric variations in the system response [9]. The objective here is to make inferences on occurrence of the evolving *slow-time-scale* faults (e.g., gradual breakdown in winding insulation), based on changes in the observed statistics of the *fast-time-scale* process (e.g., stator voltage) dynamics. The problem of pattern recognition from time series data for machine health monitoring has been recently addressed by many researchers [10,11].

Early detection of anomalies and pattern recognition have motivated formulation and validation of Symbolic Dynamic Filtering (SDF) [9,12–14]. The anomaly detection method, presented in this paper, is built upon the concept of SDF and is based on the following assumptions:

- The system behavior is stationary at the fast time scale of the process dynamics;
- An observable non-stationary behavior of the dynamical system can be associated with anomaly(ies) evolving at a slow time scale.

In the above context, stationarity pertains to statistical nature of time series data and does not imply periodic angular motion of the machine. Consequently, the first of the above two assumptions remains valid even under heavy imbalance of stator voltage and resulting vibration of the machine.

* Corresponding author.
E-mail addresses: rg_samsi@yahoo.com (R. Samsi), axr2@psu.edu (A. Ray), mayer@ee.psu.edu (J. Mayer).
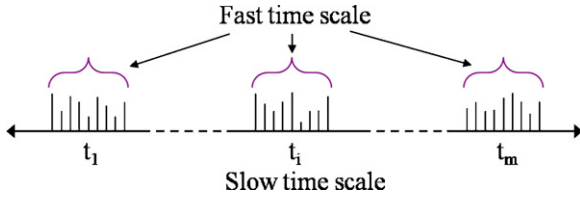
Fig. 1. Two time scales: (i) *Slow time scale* of anomaly evolution and (ii) *Fast time scale* for data acquisition and signal conditioning.

Since imbalance of stator voltage monotonically increases on the slow time scale, they can be detected from the data sequences observed on the fast time scale and the above assumptions do not limit the scope of the problem to be tackled. The framework of the anomaly detection problem consists of the following two steps.

- Preprocessing of observed time series data using wavelet analysis [15] and Parks vector representation [16];
- Pattern Classification based on the preprocessed data sets.

The paper is organized in six sections including the present one. The basic characteristics of fault signatures due to voltage imbalance are described in Section 2. Then, two parts of the above framework to detect voltage imbalance are discussed in Sections 3 and 4. The results on an experimental apparatus are presented in Secion 5 as a proof of concept for the proposed anomaly detection algorithm. Finally, the paper is concluded in Section 6 along with recommendations for future research.

2. Analysis of fault signatures

A basic analysis of the stator currents indicates that the fault information is contained in the range of twice the line frequency, which is different from the case of rotor bar faults where the fault lies in the frequency region of $2sf$ and $4sf$, where s is the slip and f is the line frequency.

The information on stator-imbalance faults is not readily discernable from the line currents, i_A, i_B and i_C, especially true for small amounts of imbalance. The Parks vector transformation [16] has been adopted to isolate and identify these fault signatures. Construction of the Parks vector from the line currents is explained below.

$$i_d = \sqrt{\frac{2}{3}} i_A - \frac{1}{\sqrt{6}} i_B - \frac{1}{\sqrt{6}} i_C \tag{1}$$

$$i_q = \frac{1}{\sqrt{2}} i_B - \frac{1}{\sqrt{2}} i_C \tag{2}$$

where i_d and i_q are the direct and quadrature axis currents respectively. These currents should ideally be $\pi/2$ radians out of phase.

$$i_d = \sqrt{\frac{3}{2}} i_M \cos(\omega t) \tag{3}$$

$$i_q = \sqrt{\frac{3}{2}} i_M \sin(\omega t) \tag{4}$$

In a parametric plot with t as the parameter, the direct and quadrature axis currents represent an ellipse.

$$i_d^2 + i_q^2 = \frac{3}{2} i_M^2 \tag{5}$$

where i_M becomes a constant under constant shaft load. The quantity in Eq. (5) is known as the Parks vector modulus [16], which may be subjected to significant deviations as a result of the supply voltage imbalance.
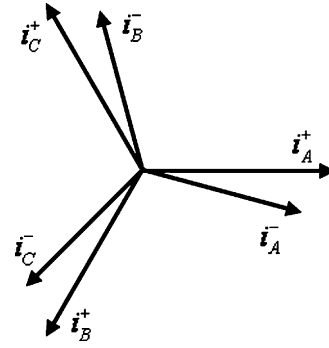

Fig. 2. Induction motor currents under imbalanced operation.

The imbalanced supply voltage causes the stator currents to be unbalanced and the unbalanced currents are represented by positive sequence and negative sequence currents,[1] i_A^+ and i_A^-; i_B^+ and i_B^-; and i_C^+ and i_C^-, as shown in Fig. 2.

Let the positive and negative sequence currents have maximum values of I_+ and I_-, respectively. Then, the three line currents are represented as follows:

$$i_A = I_+ \cos(\omega t + \varphi_+) + I_- \cos(\omega t + \varphi_-) \tag{6}$$

$$i_B = I_+ \cos\left(\omega t + \varphi_+ - \frac{2\pi}{3}\right) + I_- \cos\left(\omega t + \varphi_- - \frac{4\pi}{3}\right) \tag{7}$$

$$i_C = I_+ \cos\left(\omega t + \varphi_+ - \frac{4\pi}{3}\right) + I_- \cos\left(\omega t + \varphi_- - \frac{2\pi}{3}\right) \tag{8}$$

where φ_+ and φ_- are the phase angles of the positive and negative sequence currents, respectively. For an unbalanced condition, it follows from Eqs. (1)–(4) that the direct and quadrature axis currents are:

$$i_d = \sqrt{\frac{3}{2}} I_+ \cos(\omega t + \varphi_+) + \sqrt{\frac{3}{2}} I_- \cos(\omega t + \varphi_-) \tag{9}$$

$$i_q = \sqrt{\frac{3}{2}} I_+ \sin(\omega t + \varphi_+) - \sqrt{\frac{3}{2}} I_- \sin(\omega t + \varphi_-) \tag{10}$$

Then, following Eq. (5), the Parks vector modulus [16] becomes:

$$i_d^2 + i_q^2 = \frac{3}{2}(I_+^2 + I_-^2) + 3I_+ I_- \cos(2\omega t + \varphi_+ + \varphi_-) \tag{11}$$

The fault signature resides at twice the line frequency 2ω, which is obvious from the profiles of power spectra in Fig. 3 in the vicinity of 120 Hz.

The next two sections present the framework employed to detect voltage imbalance at an early stage. A block diagram of this procedure is shown in Fig. 4.

3. Wavelet processing of stator signals

Although models of electrical motors and drive systems are available for prediction of their normal (i.e., healthy) behavior, such models may not be adequate for identification of incipient faults due to the presence of spurious disturbances and measurement uncertainties. Therefore, a convenient way of identifying the dynamical behavior of electrical motors is to rely on both model prediction and sensor-based observation.

The need to extract relevant physical information about the observed dynamics has lead to development of nonlinear time

---

[1] For a three-wire system with a floating neutral there are no 0-sequence currents.
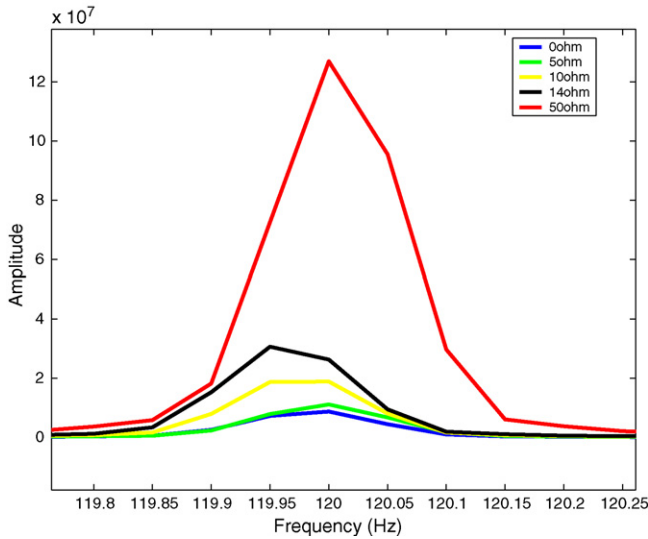
Fig. 3. Power spectral density at different levels of imbalance.

series analysis (NTSA) techniques. Identification of nonlinear systems can be achieved via *Formal Language* representation. In this paper, a discrete symbolic description is derived from the scale series obtained by wavelet analysis.

Preprocessing of the raw time series data involves data collection, followed by extraction of meaningful information. In this paper, data preprocessing is performed by wavelet analysis that yields both time and frequency information [17]. The continuous wavelet transform (CWT) has been used for data analysis which, for a function $f(t)$, is given by:

$$\text{CWT}_{\alpha,\beta} = \int_{-\infty}^{\infty} f(t)\psi^* \left(\frac{t-\tau}{\alpha}\right) dt \qquad (12)$$

where $\psi(t)$ is the wavelet basis function with $\alpha > 0$ being the scale and τ being the time shift. Hence, the wavelet transform coefficients are a function of both time and scale.

Selection of the wavelet basis function $\psi(t)$ and the scales α are crucial for robustness and performance of the fault detection methodology. If an inappropriate wavelet basis is chosen, the number of coefficients required to represent the original signal could become large. Several wavelet basis functions were tested including Haar, Gauss, and Mexican Hat [15]. All of them performed satisfac-

Fig. 4. Block diagram of the anomaly detection procedure.

torily. The Haar wavelet was chosen because of its simplicity and due to the fact that it can detect changes in the dc (i.e., constant) components in the signal easily. Although there is no known standard procedure for the choice of scales, the following guideline has proven to be useful.

For every wavelet, there exists a certain frequency called the center frequency (F_c). The pseudo-frequency f_p of the wavelet at a particular scale α is given by the following formula [15].

$$f_p = \frac{F_c}{\alpha} \qquad (13)$$

The Power Spectral Density (PSD) of a given signal or the physical knowledge of the system from which the signal is obtained to provide the information about the frequencies at which the fault signature is predominant. This information along with Eq. (13) has been used to select the scales.

Once the wavelet basis and scales are chosen, the wavelet coefficients are obtained for each of the scales. These coefficients are stacked from end to end starting with the smallest value of scale and ending with the largest value. In this paper, the wavelet coefficients versus scale at position shift τ_k are stacked after the ones at time shift τ_{k-1}, to obtain the so-called scale series data in the wavelet space [9,12].

3.1. Discretization of the wavelet space

The wavelet space is first discretized based on an appropriate Poincare section P [18]. Since the wavelet transform is linear, this is equivalent to partitioning the time series data. The resulting space of the map is divided into finitely many cells to obtain a coordinate grid for the underlying dynamics. Thus, partitioning maintains the essential behavior of the dynamical system while reducing the complexity of the problem from the continuous domain to the discrete domain and reducing the problem to a finite state representation. This is the essential feature of space partitioning that lends itself to easier pattern classification.

For simplicity, a compact set Ω within which the trajectories of the dynamical system are circumscribed, is identified with the wavelet space itself. The encoding of Ω is accomplished by introducing a partition $\mathbf{B} = (B_0, B_1, B_2, B_{n-1})$ consisting of n mutually exclusive and exhaustive subsets, i.e., $B_j \cap B_k = \emptyset, \forall j \neq k, \cup_{j=1}^{n} B_j = \Omega$. The dynamical system describes an orbit $O = (x_0, x_1, x_2, \ldots, x_n, \ldots)$, which passes through or touches various elements of the partition $\mathbf{B}$. Let us denote the index of domain $B_i \in \mathbf{B}$ visited at the time instant i as the symbol $\sigma_i \in \Sigma$. The set of symbols $\Sigma = (\sigma_1, \sigma_2, \ldots, \sigma_{n-1})$ labeling the partition elements is called the alphabet. This forms a mapping from the wavelet space to the space of symbols. Such a mapping is called Symbolic Dynamics, as it attributes a legal (i.e., physically admissible) symbol sequence to the system dynamics. As the size of each cell is finite and the cardinality of the alphabet Σ is finite, any such symbol sequence represents, through iteration, a trajectory that has the compact support Ω.

In general, a dynamical system would generate only a subset of all possible sequences of symbols as there are many illegal (i.e., physically inadmissible) sequences. The grammar (i.e., set of rules) that determines legality of symbol strings in the alphabet Σ may change with the occurrence of the fault that, as discussed earlier, occurs in the slow time scale. In essence, partitioning can be viewed as coarse graining of the wavelet space and hence subjected to (possible) loss of information. However, the essential robust features (e.g., periodic behavior or chaotic behavior of an orbit) are expected to be preserved in the symbol sequences through an appropriate partitioning of the wavelet space [19].

After the scale series data are constructed, the objective is to convert this data set into a sequence of symbols. In this uniform par-
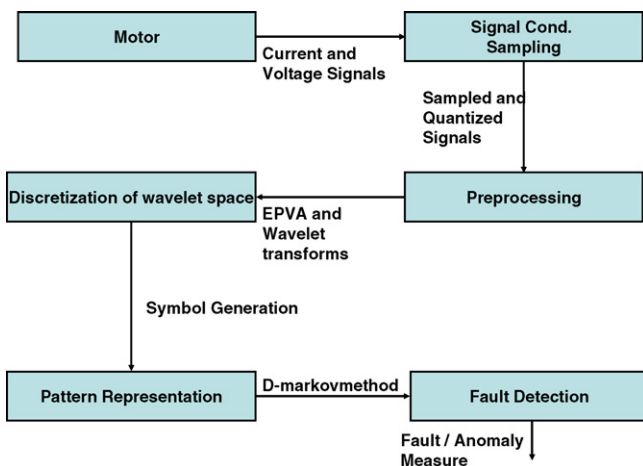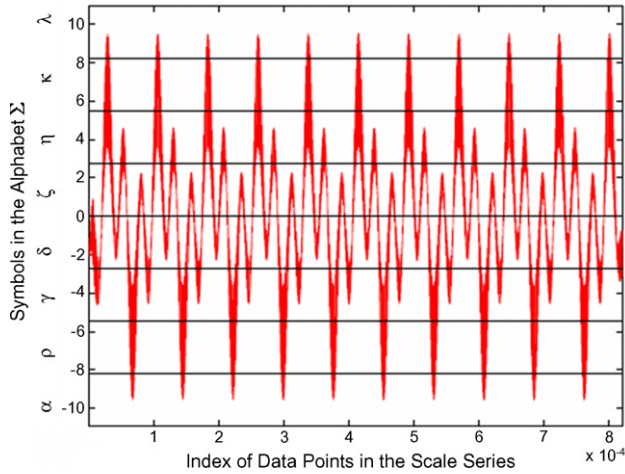
Fig. 5. Symbol generation from scale series data.

Fig. 6. Finite state machine for representation of induction motor dynamics.

titioning method, the maximum and minimum of the scale series was found. The ordinates between the maximum and minimum were split into equal-sized regions. These regions are mutually disjoint and they form a partition. Each region is associated with one symbol from the alphabet. If the data point lies in a particular region, it is coded with the symbol associated with that region. Thus, a sequence of symbols is generated from the scale series. Fig. 5 depicts the partitions and the symbols associated with them.

In this paper, the wavelet space (scale series) is partitioned into segments of equal size; this method is called *Uniform Partitioning*. Other methods such as *Maximum Entropy Partitioning* [12] are also applicable and their investigation is topic of future research.

4. Pattern classification

Having obtained the symbol sequence there arises a need to represent this pattern of symbols. This has been accomplished by using a probabilistic finite state machine, called *D*-Markov machine, in Symbolic Dynamic Filtering (SDF) [9].

4.1. D-Markov machine

The purpose of a probabilistic finite state machine is to capture the dynamical behavior of the underlying process. The core assumption in the construction of a *D*-Markov machine is that the symbolic process can be approximated, to a desired level of accuracy, as a *D* th order Markov chain and $D \in \mathbb{N}$, where $\mathbb{N}$ is the set of positive integers. The states are chosen as words of length *D* from the symbol sequence. With the cardinality $|\Sigma|$ of the alphabet and the depth *D*, the maximum number of states in the *D*-Markov machine is given by $|\Sigma|^D$. The state machine moves from one state to another upon occurrence of an event. All symbol sequences for which the last *D* symbols are the same, belong to the same equivalence class that forms a state. For $D = 1$, it becomes a regular Markov process, with each new symbol leading it to the next state. In this paper, this happens to be the case and the *D*-Markov machine is shown in Fig. 6.

Having constructed the *D*-Markov machine, the state transitional probabilities $\pi_{ij}^{(\sigma_\ell)}$ between the states, upon occurrence of the symbol $\sigma_\ell \in \Sigma$, are determined, where *i* is the state of origin and *j* is the state transitioned to. As the system trajectory evolves, different states are visited with different frequencies. The number of times a state is visited as well as the number of times a particular
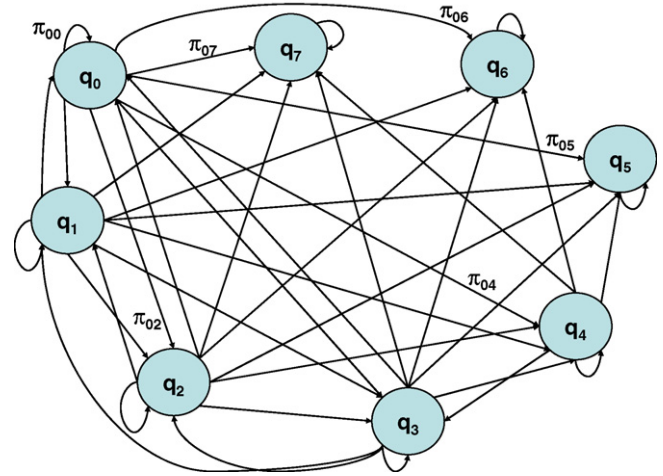
symbol is received, is counted. The state probabilities and the state-to-state transition probabilities are calculated for each state in this way. The probabilities are obtained by frequency counts based on the stopping rule reported in [20,21]. Thus, $\pi_{ij}^{(\sigma_\ell)} \approx n_i^{(\sigma_\ell)}/N_i$, where $n_i^{(\sigma_\ell)}$ is the number of times the symbol σ_ℓ occurred at the state *i* and N_i is the total number of occurrences of symbols at the state *i*, i.e $N_i = \sum_k n_i^{(\sigma_k)}$.

The matrix comprised of the transitional probabilities between the various states is called the state transition matrix $\mathbf{\Pi}$, shown in Tables 1–3. The columns of the matrices indicate the original state and the rows indicate the state transitioned to. The entries in the tables indicate the probabilities with which these transitions occur. The row sum of these $\mathbf{\Pi}$ matrices should always be unity $\mathbf{\Pi}$ is a stochastic matrix. The unity-valued entries, if any, in the matrix correspond to the states that are not visited at all, since if the machine does go into any of those states, it will not be able to exit the state.

4.2. Anomaly measure and anomaly detection

The probabilistic finite state machines, described in Section 4.1, are capable of representing patterns in the behavior of a dynamical system under faulty/anomalous conditions. In order to quantify changes in the patterns, an anomaly measure, denoted as $\mathbf{M}$, is introduced. The state transition probabilities are dependent on the underlying system dynamics as reflected in the symbol sequence. This is a factor in detecting an fault/anomaly because perturbations in the system dynamics causes significant changes in the state transition probabilities, though such changes may also be dependent on how the wavelet space is partitioned. The induced norm of the difference between the state transition matrices $\mathbf{\Pi}^0$ and $\mathbf{\Pi}$, respectively, for the nominal and anomalous state machines G^0 and G, may be used as a measure of anomaly, i.e. $\mathbf{M}(G^0, G) = ||\mathbf{\Pi}^0 - \mathbf{\Pi}||$. Alternatively, a measure of anomaly may be derived directly from state probability vector $\mathbf{p}$, whose elements denote the probability of occurrence of states of the *D*-Markov machine. This is obtained by computing the left eigenvector of the stationary $\mathbf{\Pi}$ matrix, corresponding to the unity eigenvalue [9].

Since the *D*-Markov machine has a fixed state structure, the state probability vector associated with all state machines will have the same dimension. Hence they may be used for vector representation of the anomaly, leading to the anomaly measure $\mathbf{M}(G^0, G) \triangleq ||\mathbf{p}^0 - \mathbf{p}||$.

Table 1
Π matrix for $R = 0\,\Omega$

	q_0	q_1	q_2	q_3	q_4	q_5	q_6	q_7
q_0	1.0000	0	0	0	0	0	0	0
q_1	0	1.0000	0	0	0	0	0	0
q_2	0	0	0	1.0000	0	0	0	0
q_3	0	0	0.0001	0.9475	0.0524	0	0	0
q_4	0	0	0	0.0569	0.9268	0.0163	0	0
q_5	0	0	0	0	0.2302	0.7698	0	0
q_6	0	0	0	0	0	0	1.0000	0
q_7	0	0	0	0	0	0	0	1.0000

Table 2
Π matrix for $R = 5\,\Omega$

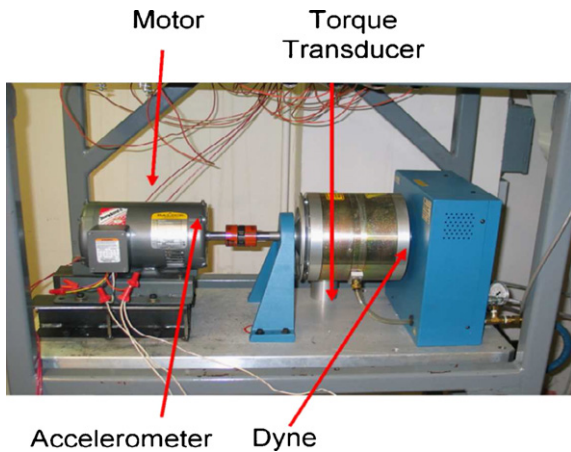|	q_0	q_1	q_2	q_3	q_4	q_5	q_6	q_7
q_0	1.0000	0	0	0	0	0	0	0
q_1	0	1.0000	0	0	0	0	0	0
q_2	0	0	0.7972	0.2028	0	0	0	0
q_3	0	0	0.0464	0.8871	0.0665	0	0	0
q_4	0	0	0	0.0611	0.9093	0.0296	0	0
q_5	0	0	0	0	0.1832	0.8168	0	0
q_6	0	0	0	0	0	0	1.0000	0
q_7	0	0	0	0	0	0	0	1.0000

Fig. 7. Laboratory test apparatus for fault detection in electric motors.

5. Experimental results and discussion

The proposed anomaly detection method has been experimentally validated on a test apparatus in the laboratory environment, which is depicted in Fig. 7. The test apparatus consists of the following components:

- *Motors*: 3-phase, 1.5 kW Y-connected squirrel cage induction motors were used. These motors are coupled using a flexible Lovejoy coupling to the dynamometer.

- *Load*: For loading the motors a hysteresis dynamometer was used, this provides two-quadrant operation. The dynamometer used was a model HD-805 6N Magtrol Inc, a hysteresis brake.
- *Sensors*: The sensor board consisted of both voltage and current sensors. The sensors have an extremely high bandwidth, they are intentionally kept that way so that high frequency as well as low frequency components harmonics could be measured and analyzed. The sensors used were LEM model numbers LV-25P and LA-55P . This is followed by operational amplifiers, realized by LM-324 IC's which provide sufficient gain. The amplified signal is sent to the data acquisition board.
- *Processor and Data Acquisition*: The data acquisition is the dSPACE Ds-1103 PPC card. This card has a Motorola Power PC 400 MHz processor. It also features sixteen 14-bit ADC units and four 12-bit ADC units, as well as eight 12-bit DAC outputs.

The stator voltage imbalance was created by adding a resistor to one of the phases of the motor. Table 1 shows the nominal **Π** matrix with no resistance added, while Tables 2 and 3 show the **Π**-matrices for imbalance with added 5 and 50 Ω, respectively. The three pairs of columns in Table 4 show the state probability vectors for three cases of 0, 5 and 50 Ω imbalance, respectively.

The added resistance was increased for every run with its values ranging from 0 to 50 Ω. In the ideal case with 0 Ω imbalance (i.e., no added resistance), the phase plot in Fig. 8 should be elliptical as indicated by Eq. (5). However, there is a noticeable distortion in the phase plots due to existence of voltage imbalance in the power supply of real-life experiments. As seen in Fig. 8, the orientation of the phase plots change monotonically with increase in resistance in one of the phases.

Table 3
Π matrix for $R = 50\,\Omega$

	q_0	q_1	q_2	q_3	q_4	q_5	q_6	q_7
q_0	0.8547	0.1094	0.0289	0.0069	0.0001	0	0	0
q_1	0.1453	0.7012	0.0956	0.0397	0.0179	0.0004	0	0
q_2	0.0473	0.1354	0.6406	0.1058	0.0434	0.0275	0	0
q_3	0.0077	0.0659	0.1181	0.6240	0.1139	0.0505	0.0200	0
q_4	0	0.0186	0.0579	0.1114	0.6263	0.1184	0.0579	0.0095
q_5	0	0	0.0174	0.0564	0.1047	0.6513	0.1335	0.0368
q_6	0	0	0	0.0089	0.0435	0.0998	0.7238	0.1240
q_7	0	0	0	0	0.0033	0.0223	0.1111	0.8632

Table 4
p vector for $R = 0$, 5 and 50 Ω

0 Ω		5 Ω		50 Ω	
q_0	0	q_0	0	q_0	0.1711
q_1	0	q_1	0	q_1	0.1338
q_2	0.0001	q_2	0.0918	q_2	0.0996
q_3	0.5033	q_3	0.4013	q_3	0.0919
q_4	0.4637	q_4	0.4365	q_4	0.0933
q_5	0.0329	q_5	0.0704	q_5	0.1042
q_6	0	q_6	0	q_6	0.1424
q_7	0	q_7	0	q_7	0.1637

The block diagram in Fig. 4 shows the procedure that was followed in the laboratory experiments. The motor was loaded to two-thirds of full load, i.e., 1.0 kW, and time series data were collected for 100 s at a sampling rate of 1 kHz. For analysis of imbalance detection, 10 s of data were used after the motor had reached steady-state operation. Tests at other load levels down to 0.5 kW were also conducted; these tests yielded similar results. The next step was online computation of the Parks vector transform and calculation of the Parks vector Modulus following Eq. (11). The mean of this modulus was subtracted from each sample to remove the DC bias. Wavelet analysis was performed on this transformed data with the basis function 'db1' [15]; the scales were chosen between 6 and 10 with a step size of 0.2, using the guidelines given earlier. The alphabet size was $|\Sigma| = 8$ and the depth was chosen to be $D = 1$.

It is seen in Tables 1–3 that the structure of Π-matrices for 0, 5, and 50 Ω changes dramatically with increase in imbalance. For example, several transitions (e.g., from q_0 to q_1) that are unlikely to occur under the nominal condition, do occur in the case of 50 Ω imbalance. There is an important observation to make in the nominal case, which is the fact that many of states have a transition probability of 1, while making transitions to themselves. These states represent very rare occurrences, but if they do occur, then the automaton stays in these deadlock states.

The norm of the difference between the nominal condition (i.e., without imbalance) and the ones with imbalance yields non-zero anomaly/fault measure. The normalized anomaly measure plot is shown in Fig. 9. For example, with a suitable threshold function (shown in the figure), it is possible to detect incipient faults early. For a similar fault, other methods like neural networks could detect a change only when the imbalance exceeded 0.2 per unit, (which is 28 Ω in this case) as reported in [22].
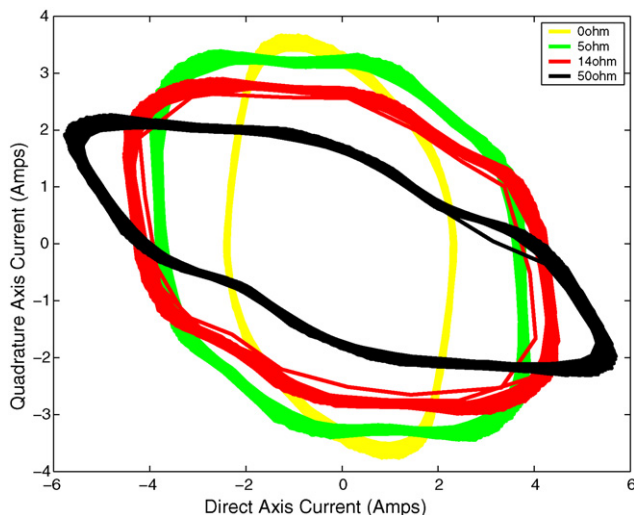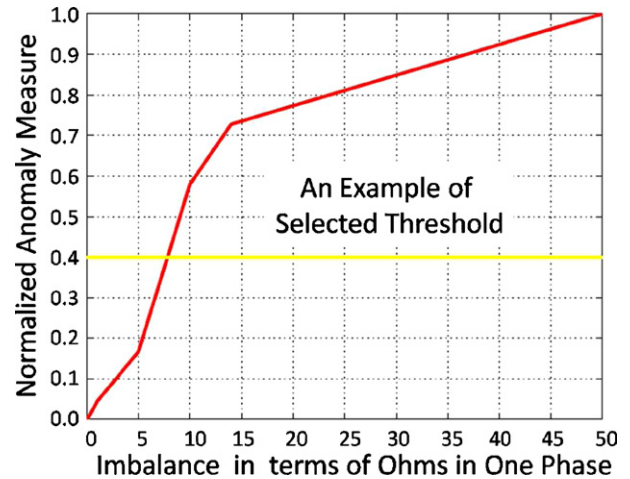

Fig. 9. Normalized anomaly measure as a function of imbalance.

One of the main advantages of the proposed SDF-based detection method is its excellent noise rejection capability because noise is filtered out in the wavelet transform and is also averaged out by repeated traverse in the D-Markov machine. The proposed method is also computationally simple as it is essentially a counting process after taking the wavelet transform.

6. Conclusions and future work

This paper presents a novel method for detecting stator voltage imbalance in three-phase induction motors. The underlying algorithm is formulated based on *Symbolic Dynamic Filtering* (SDF) that involves wavelet transform of stator current signals and subsequent analysis based on D-Markov machine construction [9]. A key advantage of the proposed method is that it is computationally less intensive than many existing anomaly detection methods and yet is capable of detecting incipient faults at an early stage.

The anomaly detection method has been experimentally validated on a 3-phase, 2-HP squirrel cage induction motor in the laboratory environment. This SDF-based anomaly detection has been shown to be successful in other applications such as fatigue damage monitoring [13,14]. Hence, it is believed that the proposed method would also be successful for fault detection in other types of electric motors (e.g., permanent-magnet machines, and reluctance machines) and electronic drive systems; ongoing research efforts are focused in this direction. Before embarking on industrial applications this anomaly detection method, further theoretical and experimental research is recommended in the following areas:

- Formulation of alternative techniques for space partitioning.
- Investigation of effects of the SDF parameters (e.g., D and $|\Sigma|$) on the performance of anomaly detection.
- Experimentation on other types of faults such as broken rotor bars and faulty bearings in the motor shaft.
- Experimentation on high performance drives, where both noise level and signal bandwidth are higher than those in standard squirrel-cage motors.
- Experimentation on with other types of electric motors and electronic drive systems.

Fig. 8. Parks vector phase plot.

References

[1] J. Kohler, J. Sottile, F. Trutt, Condition monitoring of stator windings in induction motors: Part i+–experimental investigation of the negative-sequence impedance detector, IEEE Transactions on Industry Applications 38 (5) (2002) 1447–1453.

[2] F. Trutt, C. Cruz, J. Kohler, J. Sottile, Prediction of electrical behavior in deteriorating induction motors, IEEE Transactions on Industry Applications 29 (6) (1993) 1239–1243.

[3] F. Trutt, J. Sottile, J. Kohler, Online condition monitoring of induction motors, IEEE Transactions on Industry Applications 38 (6) (2002) 1627–1632.

[4] J. Sottile, F. Trutt, J. Kohler, Condition monitoring of stator windings in induction motors: Part ii–experimental investigation of voltage mismatch detector, IEEE Transactions on Industry Applications 38 (5) (2002) 1454–1459.

[5] F. Trutt, J. Sottile, J. Kohler, Detection of ac machine winding deterioration using electrically excited vibrations, IEEE Transactions on Industry Applications 37 (1) (2001) 10–14.

[6] J. Kueck, J. Criscoe, N. Burstein, Assessment of valve actuator motor rotor degradation by fourier analysis of current waveform, IEEE Transactions on Energy Conversion 7 (3) (1992) 460–469.

[7] M.-Y. Chow, R. Sharpe, J. Hung, On the application and design of artificial neural networks for motor fault detection: Parts i and ii, IEEE Transactions on Industrial Electronics 40 (2) (1993) 189–196.

[8] P. Goode, M.-Y. Chow, Using a neural/fuzzy system to extract heuristic knowledge of incipient faults in induction motors. Part i—methodology, IEEE Transactions on Industrial Electronics 42 (2) (1995) 131–138.

[9] A. Ray, Symbolic dynamic analysis of complex systems for anomaly detection, Signal Processing 84 (7) (2004) 1115–1130.

[10] M. Eltabach, A. Charara, I. Zein, A comparison of external and internal methods of signal spectral analysis for broken rotor bars detection in induction motors, IEEE Transactions on Industrial Electronics 51 (1) (2004) 107–121.

[11] S. Cruz, H. Toliyat, A. Cardoso, Dsp implementation of the multiple reference frames theory for the diagnosis of stator faults in a dtc induction motor drive, IEEE Transactions on Energy Conversion 20 (2) (2005) 329–335.

[12] V. Rajagopalan, A. Ray, Symbolic time series analysis via wavelet-based partitioning, Signal Processing 86 (11) (2006) 3309–3320.

[13] S. Gupta, A. Ray, E. Keller, Online fatigue damage monitoring by ultrasonic measurements: a symbolic dynamics approach, International Journal of Fatigue 29 (2007) 1100–1115.

[14] S. Gupta, A. Ray, Real-time fatigue life estimation in mechanical structures, Measurement Science and Technology 18 (2007) 339–351.

[15] S. Mallat, A Wavelet Tour of Signal Processing, second ed., Academic Press, San Diego, CA, USA, 1998.

[16] P. Krause, O. Wasynczuk, S. Sudhoff, Analysis of Electric Machinery, IEEE Press, New York, NY, 1995.

[17] B. Benbouzid, G. Kliman, What stator current processing-based technique to use for induction motor rotor faults diagnosis? IEEE Transactions on Energy Conversion 18 (2003) 238–244.

[18] H. Kantz, T. Schreiber, Nonlinear Time Series Analysis, second ed., Cambridge University Press, United Kingdom, 2004.

[19] R. Badii, A. Politi, Complexity hierarchical structures and scaling in physics, Cambridge University Press, United Kingdom, 1997.

[20] A. Ray, Signed real measure of regular languages for discrete-event supervisory control, International Journal of Control 78 (12) (2005) 949–967.

[21] S. Gupta, A. Ray, A. Mukhopadhyay, Anomaly detection in thermal pulse combustors using symbolic time series analysis, Proceedings of IMechE Part I: Journal of Systems and Control Engineering 1957 (2006) 5.

[22] H. Nejjari, M. Benbouzid, Monitoring and diagnosis of induction motors electrical faults using a current park's vector pattern learning approach Electric Machines and Drives, in: International Conference IEMD '99, 9–12 May, 1999.